

**Effects of polymorphism on charge transport in organic semiconductors**Oana D. Jurchescu,<sup>1,2,\*</sup> Devin A. Mourey,<sup>2</sup> Sankar Subramanian,<sup>3</sup> Sean R. Parkin,<sup>3</sup> Brandon M. Vogel,<sup>4</sup> John E. Anthony,<sup>3</sup> Thomas N. Jackson,<sup>2</sup> and David J. Gundlach<sup>1,\*</sup><sup>1</sup>*Semiconductor Electronics Division, National Institute of Standards and Technology, Gaithersburg, Maryland 20899, USA*<sup>2</sup>*Department of Electrical Engineering, Center for Thin Film Devices and Materials Research Institute, Pennsylvania State University, University Park, Pennsylvania 16802, USA*<sup>3</sup>*Department of Chemistry, University of Kentucky, Lexington, Kentucky 40506, USA*<sup>4</sup>*Department of Chemical Engineering, Bucknell University, Lewisburg, Pennsylvania 17837, USA*

(Received 23 March 2009; revised manuscript received 8 June 2009; published 12 August 2009)

The increasing interest in fluorinated 5,11-bis(triethylsilylethynyl)anthradithiophene is motivated by the demonstrated high-performance organic field-effect transistors and circuits based on this organic semiconductor, complemented by reduced complexity processing methods that enable this performance. We identify two polymorphs of this material and report on their crystal structure, formation, and the effect of the different molecular packings on the electronic properties. The polymorphs are interconvertible through a phase transition that occurs at  $T=294$  K. We study the variations in the electrical properties as a response to the structural changes induced by the phase transition in both single crystals and thin films, and discuss the technological implications that a room-temperature phase transition has on the performance and stability of devices fabricated with this organic semiconductor.

DOI: [10.1103/PhysRevB.80.085201](https://doi.org/10.1103/PhysRevB.80.085201)

PACS number(s): 81.30.Hd, 72.80.Le, 71.20.Rv, 85.30.Tv

**I. INTRODUCTION**

Interest in organic semiconductors for electronic applications has stimulated the effort to understand and model charge transport in this class of materials<sup>1,2</sup> and to define the limits of their utility. Solution processable small-molecule organic semiconductors are particularly interesting due to their high field-effect mobilities coupled with simple processing. For small-molecule organic semiconductors, charge transport is closely related to the crystal-packing motif, which in turn is the result of the cooperation and competition of van der Waals and quadrupolar interactions between induced and permanent dipoles and multipoles (usually quadrupoles).<sup>3</sup> Owing to the weak-interaction energies, variation in the crystal packing (*polymorphism*) is frequently encountered in these materials. The formation of different polymorphs can be induced during the growth process or subsequent treatment by variations in different physical parameters. For example, in pentacene, four thin-film morphologies with characteristic interlayer separation ( $d_{001} = 14.1, 14.4, 15.1, \text{ and } 15.4 \text{ \AA}$ ) were reported.<sup>4–6</sup> The different molecular packing can be induced by control of the substrate type and temperature, as well as thickness of the film. Two types of orthorhombic rubrene [space group *Aba2* (Ref. 7) and *Cmca* (Ref. 8)] can be grown, depending on the pressure at which the material is sublimed. Polymorphism was also reported in quaterthiophene ( $\alpha-4T$ ) (Ref. 9) and sexithiophene ( $\alpha-6T$ ) (Ref. 10) for crystals grown at different source temperatures. In all aforementioned cases, the molecular arrangements are imposed during the growth process. But the polymorphism can also be driven by enantiotropic transitions, in which the crystal structure changes reversibly at a particular temperature and pressure. This type of polymorphism has been reported for pentacene<sup>11</sup> and di-indenoperylene.<sup>12</sup> Semiconducting organic crystals with different polymorphs have advantages and disadvantages. On

the one hand, they provide unique systems to understand phenomena related to the fundamental mechanism of charge transport in organic semiconductors such as the influence of the crystal packing on the electronic properties.<sup>13</sup> This is possible because with different polymorphs the chemical composition is constant and only the orientation of the constituent building blocks with respect to each is different.<sup>14</sup> On the other hand, the occurrence of different molecular-packing motifs may hamper reproducibility, stability, and reliability of devices fabricated with these materials. In order to be able to control the material properties and prevent undesired effects, it is important to know the parameter space that yields particular polymorphs and the changes expected in the electrical properties as a result of the transition to a different crystal packing.

Variations in the electronic properties of an organic semiconductor, originating from different packing of the molecules in the crystal, were predicted theoretically<sup>13,15</sup> but challenging to be experimentally demonstrated. In this paper we give experimental proof that the electrical properties of an organic crystalline semiconductor are sensitive to the different molecular arrangements and we are able to observe this effect using field-effect transistor (FET) measurements. We report on the formation and structure of two polymorphs of fluorinated 5,11-bis(triethylsilylethynyl)anthradithiophene (diF TES ADT) [see chemical structure in Fig. 1(a)] (Ref. 16) and their effect on the electronic properties and inevitably the performance of FETs fabricated from this material. This organic semiconductor has attracted increasing interest lately given its performance and unique properties.<sup>17–19</sup> Typical mobilities are in the order of  $1\text{--}6 \text{ cm}^2/\text{V s}$  in the single-crystal form<sup>20</sup> and  $0.5\text{--}1.5 \text{ cm}^2/\text{V s}$  in thin films.<sup>16,21–23</sup> While they are lower than the highest mobilities of the materials that have set the benchmarks for organic semiconductors: rubrene<sup>24–27</sup> and pentacene<sup>28</sup> but comparable to the mobility of rubrene on similar dielectrics,<sup>25</sup> diF TES ADT presents a great advan-

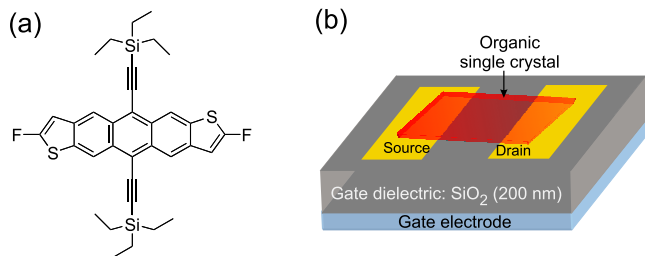


FIG. 1. (Color online) (a) Chemical structure of diF TES ADT. (b) Schematic drawing of the organic single-crystal field-effect transistors investigated in this study.

tage as its structure was engineered to be soluble in many common organic solvents and to maintain the high performance in thin-film transistors (TFTs) fabricated by solution deposition. This property facilitates compatibility with inexpensive plastic substrates and low-cost, high-volume manufacturing methods, and enables this material to be a strong candidate for large-area electronic applications.<sup>16,17,21</sup> The enhanced performance of the TFTs fabricated with diF TES ADT is partially attributed to the high crystallinity of the solution-cast films, achieved by self-patterning on chemically tailored source/drain contacts.<sup>17</sup> The presence of an enantiotropic structural phase transition enables a unique opportunity to study the effect of molecular packing on electronic properties as the two polymorphs differ only by the relative orientation of the molecules. Other parameters that may affect the charge transport such as interfacial roughness, injection barriers, or anisotropy, are identical. In this study we have investigated single crystals, as well as thin films, and we have found that the structural phase transition in diF TES ADT does not change dramatically either the molecular packing, or the electrical properties, but it may affect the long term performance of the devices.

## II. EXPERIMENT

### A. Structure determination

Differential scanning calorimetry (DSC) performed on crystals of diF TES ADT grown from solution shows the signature of a reversible phase transition at  $T_{tr}=294$  K. Complementary single crystal and powder x-ray diffraction (XRD) confirm that this is a structural phase transition, giving rise to the formation of two polymorphs. We will adopt the following nomenclature for the two polymorphs: *LT polymorph* (low-temperature polymorph, present at  $T < T_{tr}$ ) and *HT polymorph* (high-temperature polymorph, present at  $T > T_{tr}$ ). In order to obtain a detailed picture of the structural changes induced by phase transition in diF TES ADT, we performed structure determination on a single crystal grown from solution at two temperatures in the vicinity of the transition temperature:  $T=245$  K and  $T=315$  K. X-ray diffraction data were collected on a Bruker-Nonius X8 Proteum diffractometer using Cu- $K\alpha$  radiation from a rotating anode (Nonius FR591). Low-temperature data were collected on a crystal cooled to 243 K. After the low-temperature data set, the crystal was warmed to 315 K over about 5 min and a data

set was collected using the same set of scans (1485 frames, combined phi and omega scans in both low-resolution (10s per frame) and high-resolution (40s per frame) shells, sufficient to cover the unique portion of reciprocal space). The structures were solved using SHELXS and refined using SHELXL from the SHELX-97 (Ref. 29) program package. Molecular fragment editing, including the construction of a suitable disorder model was performed using the XP program of SHELXTL 5.0.<sup>29</sup> With the exception of a few minor component atoms on some of the disordered groups, the nonhydrogen atoms were refined with anisotropic displacement parameters. The majority of hydrogen atoms were found in difference-Fourier maps but some belonging to disordered groups had to be inferred. All hydrogens were subsequently placed at calculated positions and refined using an appropriate riding model. The relatively high  $R$  values for these refinements, particularly of the high-temperature structure, are largely a consequence of crystal quality.

### B. Device fabrication and characterization

For the fabrication of field-effect transistors at the surface of diF TES ADT single crystals, we used heavily doped silicon  $\langle 100 \rangle$  as the gate electrode with 200 nm thermally grown  $\text{SiO}_2$  as gate insulator. The schematic representation of the single-crystal field-effect transistors used in this study is presented in Fig. 1(b). The source and drain Ti/Au electrodes (5 nm Ti, 40 nm Au) were deposited by  $e$ -beam evaporation and patterned by photolithography and a lift-off process. The clean substrates were immersed in an 8 mol/l solution of octyltrichlorosilane in anhydrous hexadecane for 1 h, followed by rinse with chloroform and isopropanol. The single crystals were grown by physical vapor transport<sup>20</sup> and then laminated on top of the transistor structure.<sup>30,31</sup> More details on the single-crystal growth and device fabrication can be found in Ref. 20.

In parallel with single crystals, we have investigated the presence and effects of the phase transition in diF TES ADT thin films, which demonstrated very promising electrical performance as a result of enhanced crystallinity in the transistor channel induced by chemical modification of the source-drain contacts.<sup>17</sup> Structural analysis was done on films deposited on chemically treated gold as this substrate has demonstrated to give the highest degree of order.<sup>17</sup> The TFTs were fabricated as described in Ref. 21. We cleaned the gold with hot acetone, isopropanol, deionized water, and ultraviolet ozone. We then deposited a monolayer of pentafluorobenzenethiol by vapor treatment for 10 min. The diF TES ADT films were spincast in an argon environment, at room temperature from a 22 mg/ml (2 wt %) solution in chlorobenzene, using a spinning speed of 1000 rpm.

## III. RESULTS AND DISCUSSIONS

### A. Polymorphism in diF TES ADT

Both diF TES ADT polymorphs are layered structures (see the molecular packing in Fig. 2) and crystallize in a triclinic cell, space group  $P\bar{1}$ . The thermal expansion between the temperatures of interest ( $T=245$ – $315$  K) is aniso-

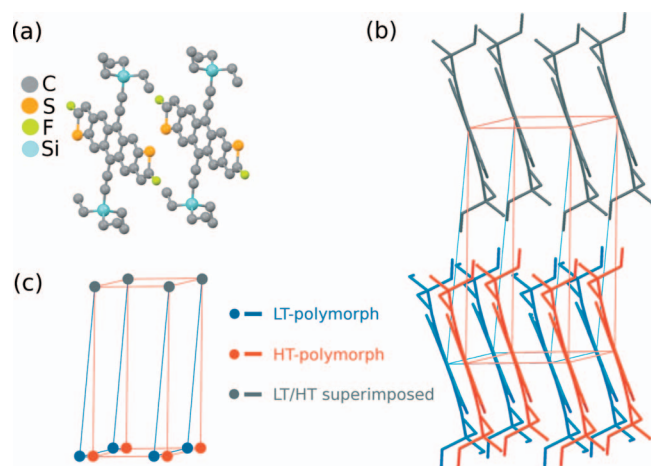


FIG. 2. (Color) (a) Cofacial packing of diF TES ADT molecules in the crystal. The constituent atoms are indicated in the legend. (b) Molecular packing for the LT (blue) and HT (red) polymorphs. The first layers of the two polymorphs are shown in dark gray and superimposed. The unit-cell axis are also indicated. The relative shift in the second layers in the  $ab$  plane is a result of the structural phase transition. (c) Simplified version of Fig. 2(b), in which only the centers of molecules, represented by circles, are indicated.

tropic ( $\Delta a=1.3\%$ ,  $\Delta b=1.1\%$ , and  $\Delta c=-1.6\%$ ), and reveals an expansion along  $a$  and  $b$  crystallographic directions and contraction along the  $c$  axis. Details on the unit-cell parameters for the two polymorphs are summarized in Table I. Complete experimental details and refinement results can be found in the supplemental files accompanying this manuscript.<sup>32</sup>

Figure 2 displays a graphical representation of the molecular packing in diF TES ADT crystals. The molecules are cofacially packed [Fig. 2(a)], in a two-dimensional  $\pi$  stack.<sup>16</sup> Figure 2(b) shows the two polymorphs, superimposed to facilitate depiction of the differences between the two structures. The first layers of the two polymorphs are overlaid (molecules shown in dark gray). The color legend that we use for the second layer is blue for the LT polymorph and red for the HT polymorph. The relative differences in molecular packing in the second layer as well as the changes in the unit cell can be easily noticed. The change in the tilt of the plane

TABLE I. Crystallographic information on the two diF TES ADT polymorphs.

$T$ (K)	LT-polymorph 245	HT-polymorph 315
$a$ (Å)	7.1153(14)	7.2089(10)
$b$ (Å)	7.2342(14)	7.3170(11)
$c$ (Å)	16.626(3)	16.352(2)
$\alpha$ (°)	97.522(9)	87.718(9)
$\beta$ (°)	91.361(9)	89.993(9)
$\gamma$ (°)	107.491(10)	71.940(8)
$V$ (Å <sup>3</sup> )	807.402	819.315
$d_{001}$ (Å)	16.4	16.3

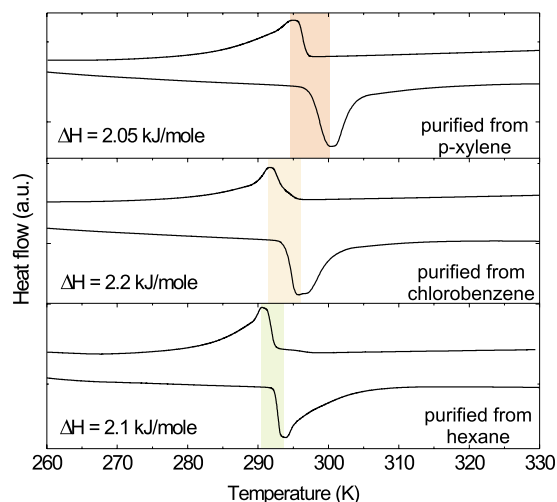


FIG. 3. (Color online) DSC spectra measured on diF TES ADT crystals grown from different solvents. The solvent name and latent heat are also indicated as an inset in each graph. The measurements are performed during heating and cooling.

of the long molecular axis (ADT core) of the molecule is very small and we will neglect it here. We describe the differences in the structure of the two polymorphs in terms of interlayer and intralayer shifts, giving rise to a weak distortion of the unit cell. The transition involves a horizontal shift in the second layer with respect to the first by  $\sim 1.45$  Å along the  $a+b$  crystallographic direction and stabilization of the structure through a vertical shift by  $\sim 0.1$  Å along the  $c^*$  direction. Figure 2(c) is a simplified version of Fig. 2(b), in which only the center of molecules is represented. The relative shift in the second layers in the  $ab$  plane can be easily observed. The vertical shift (along  $c^*$ ) gives rise to a decrease in the interplanar distance, from  $d_{001}(\text{LT})=16.4$  Å in the LT polymorph to  $d_{001}(\text{HT})=16.3$  Å in the HT polymorph. The small changes in the crystal structure agree well with the small value of the latent heat involved in the transition:  $\Delta H=2.11 \pm 0.07$  kJ mol<sup>-1</sup> (see Fig. 3).

## B. Mechanism of phase transition

We believe that the enantiotropic phase transition in diF TES ADT occurs via a nucleation and growth mechanism that promotes the coexistence of the two polymorphs over a temperature interval, as described by Herbststein for a variety of compounds.<sup>33</sup> This dynamic seems to be more general for structural phase transitions in molecular crystals. Similar effects were reported for pentacene<sup>11</sup> and di-indenoperylene.<sup>12</sup> It was suggested that in these systems the nucleation of one polymorph proceeds from defects of the other polymorph, thus the phase transformation is governed by defect density, grain size, and thermal history. As the crystal structure of the two polymorphs is not very different, single polymorph domains can coexist without dramatically distorting the crystal environment but they will inevitably introduce stress/strain fields along the domain boundaries. The coexistence of the two phases over a wide temperature interval was assumed to be responsible for the challenges encountered in detecting

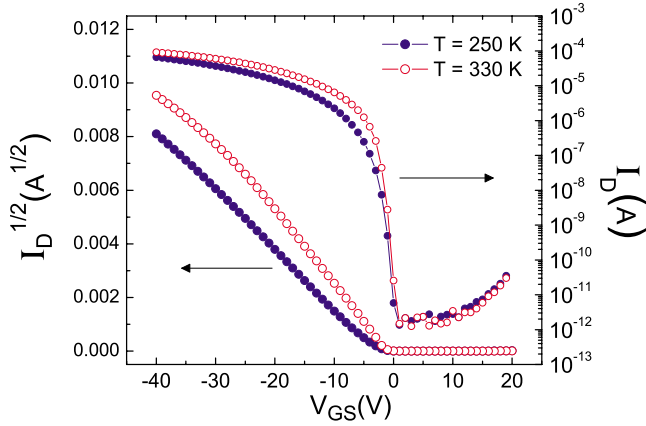


FIG. 4. (Color online) Evolution of the drain current  $I_D$  with the gate voltage  $V_{GS}$  for a diF TES ADT single-crystal FET at  $V_{DS} = -40$  V. *Right axis:*  $\log(I_D)$  vs  $V_{GS}$ . *Left axis:*  $\sqrt{I_D}$  vs  $V_{GS}$ . The data in blue is taken at  $T = 250$  K and corresponds to LT polymorph, and the plot in red is taken at  $T = 330$  K and corresponds to HT polymorph. The transistor geometry is  $L = 100$   $\mu\text{m}$ ,  $W = 500$   $\mu\text{m}$ , and the oxide thickness is  $t_{ox} = 200$  nm.

the signature of a thermal event in pentacene using DSC,<sup>11</sup> as well as for the broadening of the DSC signal in di-indenoperylene.<sup>12</sup> In the case of diF TES ADT phase transition, the DSC peaks are much better defined but the presence of a small hysteresis and temperature shift is still noticeable, as seen in Fig. 3. Here we present DSC measurements on crystals purified from different solvents (p-xylene, chlorobenzene, and hexane). The measurements are performed during heating and cooling. A rate of 5 K/min was used in all experiments. The value of the hysteresis varies from 5 K in the case of p-xylene to 3 K in the case of hexane, with overall hysteresis of  $\Delta T \approx 10$  K. We assign these variations in the transition temperature to different defect densities and spatial distribution, as well as perhaps variation in the crystalline size. The different habit of nucleation sites promotes different conversion rates. Even for crystals grown from the same solvent, the results are sensitive to the sample thermal history, consistent with the theory of nucleation-dependent phase transition.

### C. Electronic response to structural changes

Further we were interested in the electronic response to structural changes in diF TES ADT. In order to investigate the effect of the crystal packing on the electronic properties, we fabricated FETs at the surface of single crystals and thin films. We have measured the evolution of the electrical properties our FETs with temperature and found that the structural changes induced by the phase transition have direct impact on the electrical properties of the devices fabricated with diF TES ADT. Figure 4 shows the current-voltage characteristics of one of the single-crystal device investigated in this study. The data plotted in blue filled circles are taken at  $T = 250$  K and corresponds to LT-polymorph electrical properties. The data plotted in red open circles are taken at  $T = 330$  K and corresponds to HT-polymorph electrical properties. On the right axis we plot the drain current  $\log(I_D)$  as a

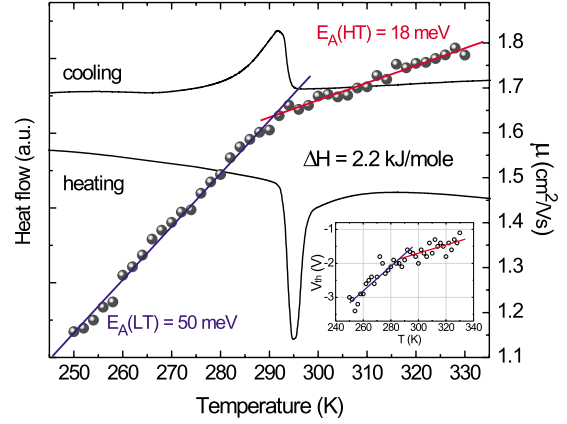


FIG. 5. (Color online) *Left axis:* DSC spectrum of diF TES ADT, showing the presence of a reversible phase transition. *Right axis:* The evolution of the field-effect mobility ( $\mu$ ) with temperature confirms the effect of the presence of the phase transition on the properties of the devices. The inset shows the changes in the threshold voltage  $V_{th}$  with temperature.

function of  $V_{GS}$  (the gate-source voltage) for the drain-source voltage  $V_{DS} = -40$  V and on the left axis we show  $\sqrt{I_D}$  vs  $V_{GS}$ . The device geometry is  $W/L = 500/100$  and the  $\text{SiO}_2$  dielectric thickness is 200 nm. The behavior at the two extreme temperatures of interest for this study is similar and shows very sharp turn on in the weak accumulation region. The differences come from different values of mobilities ( $\mu$ ) at the two temperatures as well as shifts in the threshold voltages ( $V_{th}$ ). We will discuss in more detail these two parameters later. Note the small values of  $V_{th}$  as a result of low trap densities at the interface between the gate insulator and the organic semiconductor. Thin films show similar trends but slower turn on, lower mobilities, and higher threshold voltages, strongly depended on the microstructure.<sup>21</sup> A detailed comparative description of the thin-film devices versus single-crystal devices was reported elsewhere.<sup>20,21</sup>

We have extracted the mobility  $\mu$  in the saturation regime from the slope of Fig. 4, left axis, using the standard current-voltage relationship

$$I_D = \frac{W C_i}{L} \frac{\mu}{2} (V_{GS} - V_{th})^2, \quad (1)$$

where  $C_i$  is the gate oxide capacitance per unit area, and  $W$  and  $L$  are the channel width and length, respectively. The evolution of the value of mobility for a single-crystal field-effect transistor versus temperature is plotted in Fig. 5 (right axis). The field-effect mobility responds to the phase transition by a change in slope at the same temperature where the DSC predicts the presence of a phase transition ( $T = 294$  K), see the DSC measurements on the left axis in Fig. 5. We have measured 14 single-crystal devices and have observed similar behavior. The evolution of the mobility of each polymorph with temperature shows activated behavior with different activation energies corresponding to each polymorph:  $E_A(\text{LT}) \approx 50$  meV and  $E_A(\text{HT}) \approx 18$  meV for this particular device. The subtle structural differences between the two polymorphs are reflected in a different tem-

perature activated behavior of the mobility for the two polymorphs. We interpret this temperature dependence of the mobility as an evidence for the electronic response to the structural changes.

The activated behavior of mobility in our organic single-crystal FETs seems to contradict the conventional models developed for charge transport in high-purity molecular crystals.<sup>34–36</sup> This intriguing behavior has been observed previously for other single crystals and attributed to the coupling of the charge carriers with the polar environment at the semiconductor/dielectric interface (formation of Fröhlich polarons).<sup>25,26,37</sup> Polarization effects at the dielectric-organic-semiconductor interface, as well as fluctuation of the polarization can represent sources of disorder in our FETs and may result in charge localization<sup>38</sup> and, consequently, temperature activated behavior. Additionally, in diF TES ADT the thermal vibrations<sup>39</sup> are stronger than in rubrene or pentacene. They tend to couple to the charge carriers giving rise to localization of pure coherent states and loss of coherent transport. Moreover, when the material experiences the phase transition, localization may occur via reorganization of the interface trap energy distribution.<sup>40,41</sup> This is also reflected in the threshold-voltage shift when the system passes through the transition (see the inset in Fig. 5). This shift can be assigned to charge trapping into states generated by structural changes induced by the phase transition. The different activation energies in the LT and HT polymorphs may, in part, be the result of different interactions with the substrate, different intrinsic phonon energies associated with the two crystal structures, and different trap densities. We cannot exclude a contribution from variation in the contact resistance to the total changes in the device properties but we minimize these contributions by extracting the mobility from the saturation regime. The linear regime mobility also responds to the phase transition at 294 K by a change in slope but it has lower values ( $0.6 \text{ cm}^2/\text{V s}$  at 250 K and  $1.4 \text{ cm}^2/\text{V s}$  at 330 K) and higher activation energies [ $E_A(\text{LT}) \approx 105 \text{ meV}$  and  $E_A(\text{HT}) \approx 45 \text{ meV}$  for this particular device]. The lower values of mobility, as well as the higher activation energies, may come from contact effects, as well as from fast-trapping events that dominate the linear regime.<sup>40</sup> In general, in FETs charge trapping at the organic-semiconductor/dielectric interfaces and contacts effects are not negligible. Therefore we are able to observe signature of the phase transition with our measurements but we cannot connect directly the crystal packing with electrical properties. Further time-of-flight and space-charge limited current measurements are needed to describe the effect of the phase transition on the bulk properties of diF TES ADT. Also, electronic-structure calculations are needed to discern how the changes in the crystal structure modulate the band structure of diF TES ADT and along which crystallographic directions the effect of the phase transition is most pronounced.

To study the consequences that the presence of a phase transition has on the properties of the devices relevant for technological applications, we perform a critical survey on the structural changes in a thin film similar to the film in the channel of the TFTs and correlate the results with the electrical measurements. We have previously demonstrated that single crystals grown from vapor exhibit the same crystal

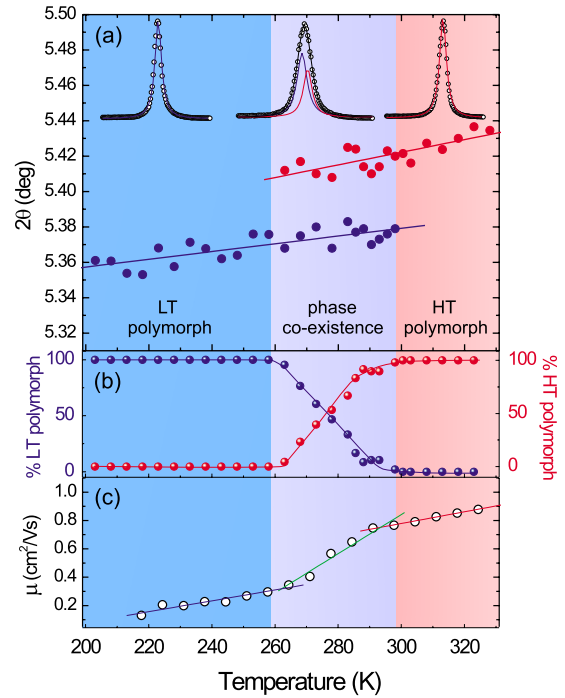


FIG. 6. (Color online) (a) Evolution of the (001) peak position for the LT polymorph (blue) and HT polymorph (red). The insets represent typical peak fits. (b) Evolution of the concentration of LT polymorph (blue) and HT polymorph (red). The phase coexistence region can be observed. (c) Evolution of the diF TES ADT thin-film transistor field-effect mobility with temperature.

structure as crystals grown from solution.<sup>20</sup> It is particularly noteworthy that XRD performed on thin films deposited from chlorobenzene, the solvent that gives the best device performance,<sup>16</sup> reveals the existence of the same polymorphs in thin films and shows signature of the presence of the structural phase transition. This observation is important as it demonstrates that the phase transition has direct implications on electronic applications fabricated with films of this material by solution deposition.

X-ray diffraction data on the film were acquired between 200 and 330 K, on a powder diffractometer, during heating. The patterns indicate the film is highly crystalline with the molecules displaying a preferred (001) orientation and adopting a packing similar to single-crystal diF TES ADT (*ab* plane parallel to the substrate). Detailed analysis of the thin-film microstructure was reported elsewhere.<sup>17</sup> From the position of the 001 peak we can estimate the interlayer separation ( $d_{001}$ ) and identify the two diF TES ADT polymorphs by their characteristic spacing. We recall the parameters that define the polymorphs:  $d_{001,\text{LT}} = 16.4 \text{ \AA}$  [ $2\Theta_{\text{LT}}(001) = 5.37^\circ$ ] and  $d_{001,\text{HT}} = 16.3 \text{ \AA}$  [ $2\Theta_{\text{HT}}(001) = 5.41^\circ$ ]. We extract the position of 001 peak for each temperature investigated in this study and we plot the results in Fig. 6(a). In blue we show the evolution of the (001) peak position for the LT polymorph and in red for the HT polymorph. Fitting the data reveals a rich phase diagram, with three regimes, as a function of temperature, including two single polymorphs regimes and one regime defined by the coexistence of the two polymorphs over a broad temperature range, with a gradual

conversion of one phase into the other. We believe the kinetics of the phase transition is controlled by the sample quality (defect density) and thermal history. This accounts for the differences in the temperature window when the phases coexist,<sup>33</sup> similar to the transitions encountered in pentacene<sup>11</sup> and di-indenoperylene.<sup>12</sup> For this film, at  $T < 263$  K the sample contains only the LT polymorph. This is confirmed by modeling the data using a single peak [see the inset in Fig. 6(a)], which shows monotonic changes in the position [Fig. 6(a), in blue]. In the temperature interval  $T = (263-298)$  K the graph displays the coexistence of both polymorphs. By comparing the peak areas in the phase coexistence regime, we can extract information about the content of each of the two polymorph and conversion rate/dynamics of the LT polymorph into the HT polymorph. As seen in Fig. 6(b), the LT polymorph gradually transforms into the HT polymorph, over a 30 K temperature window for this sample. At  $T=298$  K the conversion of LT polymorph into HT polymorph is complete and for  $T > 298$  K diF TES ADT is a one phase system. The occurrence of the phase coexistence regime, as well as the fact that the crystal symmetry does not change, suggest that this is a first-order phase transition. The phase coexistence regime is smeared over a broader temperature interval in thin film than in the single crystals. Considering the *nucleation and growth* mechanism proposed for the phase transition, these differences can be attributed to the smaller grain size present in the films, similar to the case of pentacene<sup>11</sup> and di-indenoperylene<sup>12</sup> but also the coupling to the dielectric surface, which is more severe in thin films than in thick single crystals.

Comparing the temperature dependence of the mobility [Fig. 6(c)] with the conversion of one polymorph into the other one [Fig. 6(b)], we note that the transition between the LT polymorph and the phase coexistence regime, as well as the transition from the coexistence regime to the HT polymorph are accompanied by clear changes in slope in the  $\mu(T)$  plot. The afore mentioned structural regimes present in diF TES ADT thin films are reflected in three distinct regimes in the electrical properties. Note that in thin films the electrical properties are dominated by grain boundaries,<sup>42</sup> thus the mobility is lower than the mobility in single crystals (Fig. 5). Nevertheless, we can detect the effects associated with the presence of two different polymorphs even in thin-

film transistors fabricated on diF TES ADT. However, while in single-crystal devices the effect of the phase transition on the electronic properties is clear and reproducible (all 14 devices investigated showed signature of the transition in electrical measurements at  $294 \pm 3$  K), the detection of the transition in TFTs was more challenging. This is due to the spread in the temperature window in which the LT and HT phases coexist, as a result of the presence of grain boundaries and coupling with the dielectric.

The presence of a structural phase transition around room temperature has direct implications on the technological appeal of this material. We would like to emphasize that while the enantiotropic transition in diF TES ADT does not dramatically distort its structure and electronic properties, it may be an issue for the long-term stability of the devices. While the applications based on this material<sup>22</sup> operate at room temperature, because of small environmental temperature variations diF TES ADT may undergo the polymorphic transformation multiple times and the molecular layers will repeatedly glide with respect to each other. This may give rise to stress/strain fields that may promote formation of defects, leading to performance deterioration.

#### IV. CONCLUSIONS

In conclusion, we demonstrate that fluorinated 5,11-bis(triethylsilylethynyl) anthradithiophene is an enantiotropic system near room temperature. We use the unique opportunity of the existence of two polymorphs that are interconvertible via temperature and show that subtle variations in the molecular packing drive consistent differences in the electronic properties giving rise to measurable effects in the performance of field-effect transistors. An understanding of the physical parameters that affect this thermal event is important for optimal control and manipulation of the processing and stability of devices fabricated with this and similar materials.

#### ACKNOWLEDGMENTS

We acknowledge B. Hamadani and O. Kirillov for the prefabricated substrates and Nichole Wonderling for the assistance with the low-temperature XRD.

\*Corresponding author.

†oana.jurchescu@nist.gov

‡david.gundlach@nist.gov

<sup>1</sup>M. E. Gershenson, V. Podzorov, and A. F. Morpurgo, *Rev. Mod. Phys.* **78**, 973 (2006).

<sup>2</sup>P. B. Paramonov, V. Coropceanu, and J.-L. Bredas, *Phys. Rev. B* **78**, 041403(R) (2008).

<sup>3</sup>C. A. Hunter and J. K. M. Sanders, *J. Am. Chem. Soc.* **112**, 5525 (1990).

<sup>4</sup>C. C. Mattheus, A. B. Dros, J. Baas, A. Meetsma, J. L. de Boer, and T. T. M. Palstra, *Acta Crystallogr., Sect. C: Cryst. Struct. Commun.* **57**, 939 (2001).

<sup>5</sup>C. C. Mattheus, G. A. de Wijs, R. A. de Groot, and T. T. M. Palstra, *J. Am. Chem. Soc.* **125**, 6323 (2003).

<sup>6</sup>A. Brillante, I. Bilotti, R. G. Della Valle, E. Venuti, M. Masino, and A. Girlando, *Adv. Mater. (Weinheim, Ger.)* **17**, 2549 (2005).

<sup>7</sup>D. E. Henn, W. G. Williams, and D. J. Gibbons, *J. Appl. Crystallogr.* **4**, 256 (1971).

<sup>8</sup>O. D. Jurchescu, A. Meetsma, and T. T. M. Palstra, *Acta Crystallogr., Sect. B: Struct. Sci.* **62**, 330 (2006).

<sup>9</sup>T. Siegrist, C. Kloc, R. A. Laudise, H. E. Katz, and R. C. Haddon, *Adv. Mater. (Weinheim, Ger.)* **10**, 379 (1998).

<sup>10</sup>L. Antolini, G. Horowitz, F. Kouki, and F. Garnier, *Adv. Mater. (Weinheim, Ger.)* **10**, 382 (1998).

- <sup>11</sup>T. Siegrist, C. Besnard, S. Haas, M. Schiltz, P. Pattison, D. Chernyshov, B. Batlogg, and C. Kloc, *Adv. Mater. (Weinheim, Ger.)* **19**, 2079 (2007).
- <sup>12</sup>M. A. Heinrich, J. Pflaum, A. K. Tripathi, W. Frey, M. L. Steigerwald, and T. Siegrist, *J. Phys. Chem. C* **111**, 18878 (2007).
- <sup>13</sup>A. Troisi and G. Orlandi, *J. Phys. Chem. B* **109**, 1849 (2005).
- <sup>14</sup>S. Haas, A. F. Stassen, G. Schuck, K. P. Pernstich, D. J. Gundlach, B. Batlogg, U. Berens, and H.-J. Kirner, *Phys. Rev. B* **76**, 115203 (2007).
- <sup>15</sup>H. Yoshida and N. Sato, *Phys. Rev. B* **77**, 235205 (2008).
- <sup>16</sup>S. Subramanian, S. K. Park, S. R. Parkin, V. Podzorov, T. N. Jackson, and J. E. Anthony, *J. Am. Chem. Soc.* **130**, 2706 (2008).
- <sup>17</sup>D. J. Gundlach, J. E. Royer, S. K. Park, S. Subramanian, O. D. Jurchescu, B. H. Hamadani, A. J. Moad, R. J. Kline, L. C. Teague, O. Kirillov, C. A. Richter, J. G. Kushmerick, L. J. Richter, S. R. Parkin, T. N. Jackson, and J. E. Anthony, *Nature Mater.* **7**, 216 (2008).
- <sup>18</sup>R. Hamilton, J. Smith, S. Ogier, M. Heeney, J. E. Anthony, I. McCulloch, J. Veres, D. D. C. Bradley, and T. D. Anthopoulos, *Adv. Mater. (Weinheim, Ger.)* **21**, 1166 (2009).
- <sup>19</sup>J. Day, A. D. Platt, S. Subramanian, J. E. Anthony, and O. Ostroverkhova, *J. Appl. Phys.* **105**, 103703 (2009).
- <sup>20</sup>O. D. Jurchescu, S. Subramanian, R. J. Kline, J. E. Anthony, T. N. Jackson, and D. J. Gundlach, *Chem. Mater.* **20**, 6733 (2008).
- <sup>21</sup>O. D. Jurchescu, B. H. Hamadani, H. D. Xiong, S. K. Park, S. Subramanian, N. M. Zimmerman, J. E. Anthony, T. N. Jackson, and D. J. Gundlach, *Appl. Phys. Lett.* **92**, 132103 (2008).
- <sup>22</sup>S. K. Park, D. A. Mourey, S. Subramanian, J. E. Anthony, and T. N. Jackson, *IEEE Electron Device Lett.* **29**, 1004 (2008).
- <sup>23</sup>S. K. Park, D. A. Mourey, S. Subramanian, J. E. Anthony, and T. N. Jackson, *Appl. Phys. Lett.* **93**, 043301 (2008).
- <sup>24</sup>V. Podzorov, E. Menard, A. Borissov, V. Kiryukhin, J. A. Rogers, and M. E. Gershenson, *Phys. Rev. Lett.* **93**, 086602 (2004).
- <sup>25</sup>I. N. Hulea, S. Fratini, H. Xie, C. L. Mulder, N. N. Iossad, G. Rastelli, S. Ciuchi, and A. F. Morpurgo, *Nature Mater.* **5**, 982 (2006).
- <sup>26</sup>Y. Xia, J. H. Cho, J. Lee, P. P. Ruden, and C. D. Frisbie, *Adv. Mater. (Weinheim, Ger.)* **21**, 2174 (2009).
- <sup>27</sup>J. Takeya, M. Yamagishi, Y. Tominari, R. Hirahara, Y. Nakazawa, T. Nishikawa, T. Kawase, T. Shimoda, and S. Ogawa, *Appl. Phys. Lett.* **90**, 102120 (2007).
- <sup>28</sup>O. D. Jurchescu, M. Popinciuc, B. J. van Wees, and T. T. M. Palstra, *Adv. Mater. (Weinheim, Ger.)* **19**, 688 (2007).
- <sup>29</sup>G. M. Sheldrick, *Acta Crystallogr., Sect. A: Found. Crystallogr.* **64**, 112 (2008).
- <sup>30</sup>R. W. I. de Boer, T. M. Klapwijk, and A. F. Morpurgo, *Appl. Phys. Lett.* **83**, 4345 (2003).
- <sup>31</sup>J. Takeya, C. Goldmann, S. Haas, K. P. Pernstich, B. Ketterer, and B. Batlogg, *J. Appl. Phys.* **94**, 5800 (2003).
- <sup>32</sup>See EPAPS Document No. E-PRBMDO-80-065928 for the supplemental files. For more information on EPAPS, see <http://www.aip.org/pubservs/epaps.html>.
- <sup>33</sup>F. H. Herbstein, *Acta Crystallogr., Sect. B: Struct. Sci.* **62**, 341 (2006).
- <sup>34</sup>K. C. Kao and W. Hwang, *Electrical Transport in Solids* (Pergamon, New York, 1981), Vol. 14.
- <sup>35</sup>A. Troisi and G. Orlandi, *Phys. Rev. Lett.* **96**, 086601 (2006).
- <sup>36</sup>H. A. v. Laarhoven, C. F. J. Flipse, M. Koeberg, M. Bonn, E. Hendry, G. Orlandi, O. D. Jurchescu, T. T. M. Palstra, and A. Troisi, *J. Chem. Phys.* **129**, 044704 (2008).
- <sup>37</sup>S. Ciuchi and S. Fratini, *Phys. Rev. B* **79**, 035113 (2009).
- <sup>38</sup>J.-D. Picon, M. N. Bussac, and L. Zuppiroli, *Phys. Rev. B* **75**, 235106 (2007).
- <sup>39</sup>A. Troisi, G. Orlandi, and J. E. Anthony, *Chem. Mater.* **17**, 5024 (2005).
- <sup>40</sup>C. Goldmann, C. Krellner, K. P. Pernstich, S. Haas, D. J. Gundlach, and B. Batlogg, *J. Appl. Phys.* **99**, 034507 (2006).
- <sup>41</sup>J. H. Kang, D. da Silva Filho, J.-L. Bredas, and X.-Y. Zhu, *Appl. Phys. Lett.* **86**, 152115 (2005).
- <sup>42</sup>L. C. Teague, B. H. Hamadani, O. D. Jurchescu, S. Subramanian, J. E. Anthony, T. N. Jackson, D. J. Gundlach, and J. G. Kushmerick, *Adv. Mater. (Weinheim, Ger.)* **20**, 4513 (2008).